Structural changes of synthetic paulingite (Na,H-ECR-18) upon dehydration and CO2 adsorption

Alex G. Greenaway, Jiho Shin, Paul A. Cox, Elenica Shiko, Stephen P. Thompson, Stefano Brandani, Suk Bong Hong and Paul A. Wright*

Structural changes of synthetic paulingite (Na,H-ECR-18) upon dehydration and CO_2 adsorption

Abstract: The structure of dehydrated calcined ECR-18, synthetic paulingite, topology type PAU, unit cell composition $Na_{132}H_{28}Si_{512}Al_{160}O_{1344}$, has been determined by Rietveld refinement against synchrotron X-ray powder diffraction data. Upon dehydration the symmetry of Na,H-ECR-18 changes from $Im\bar{3}m$ to $I\bar{4}3m$, with a corresponding decrease of cubic unit cell a parameter from 34.89412(1) Å to 33.3488(3) Å. This occurs as the framework distorts to afford closer coordination of Na^+ cations by framework O atoms in 8-ring window sites of the seven cage types present. Na^+ cations in 8R sites block the access of N_2 molecules to the internal pore space at 77 K but CO_2 adsorption at 308 K is observed, and is postulated to occur via a 'trapdoor' mechanism. In situ PXRD during CO_2 adsorption at pressures up to 10 bar show reversible broadening of diffraction peaks that is attributed to local crystallographic strain.

Keywords: carbon dioxide adsorption; cation locations; dehydrated structure; synthetic paulingite; trapdoor zeolite.

DOI 10.1515/zkri-2014-1824
Received November 26, 2014; accepted February 9, 2015; published online March 18, 2015

***Corresponding author: Paul A. Wright,** EaStCHEM School of Chemistry, University of St Andrews, St. Andrews, KY16 9ST, UK, E-mail: paw2@st-andrews.ac.uk
Alex G. Greenaway: EaStCHEM School of Chemistry, University of St Andrews, St. Andrews, KY16 9ST, UK
Jiho Shin and Suk Bong Hong: Center for Ordered Nanoporous Materials Synthesis, School of Environmental Science and Engineering, POSTECH, Pohang 790-784, Korea
Paul A. Cox: School of Pharmacy and Biomedical Sciences, University of Portsmouth, Portsmouth, PO1 2DT, UK
Elenica Shiko and Stefano Brandani: School of Engineering, University of Edinburgh, Sanderson Building, The King's Buildings, Mayfield Road, Edinburgh, EH9 3JL
Stephen P. Thompson: Diamond Light Source, Harwell Science and Innovation Campus, Didcot, OX11 0DE

Introduction

The selective adsorption of CO_2 from post-combustion flue gases and pre-combustion gas streams in power plants is an important requisite for future carbon capture technologies using solid adsorbents [1, 2]. Similarly, the separation of CO_2 from light hydrocarbons is important for natural gas upgrading [3]. Among the different materials proposed for these tasks, zeolites have considerable potential, if the gas streams can be prepared with low water contents. Typically, moderate selectivity for CO_2 over N_2 or CH_4 can be achieved over cationic zeolites such as Na–X [4] or Na–A [5], which result from the quadrupole moment of CO_2 and its polarisability. Recently, however, small pore zeolites of specific structures and compositions have been found to show very high selectivity for CO_2 over less polar gases such as CH_4 and N_2 due to a molecular 'trapdoor' effect that makes them strong candidates as sorbents for carbon capture [6–12].

These 'trapdoor' zeolites possess framework structures in which large cages are connected by narrow windows delimited by eight-membered rings (8Rs). They can be prepared with sufficiently high framework Al contents that charge-balancing extra-framework cations fully occupy these 8R window sites. Whereas these 'gatekeeper' cations can block diffusion of weakly interacting molecules (N_2, CH_4) between cages, and so prevent their adsorption into the pores, it is found that CO_2 is readily taken up. This is attributed to strong interaction of the 8R cations with CO_2 molecules, allowing them to move away from the windows and permit CO_2 molecules to pass (Figure 1). This mechanism allows the separation of molecules that interact strongly with cations from those adsorbates that have much weaker interactions, and so can give very high selectivity for adsorption of CO_2 over N_2 or CH_4. The separation depends on the strength of the chemical interaction rather than the molecular size and should not be considered as molecular sieving.

The trapdoor effect has been reported for zeolites with cations in single 8R window sites (S8R) and double 8R window sites (D8R) between large cages. Whereas Na,K–A

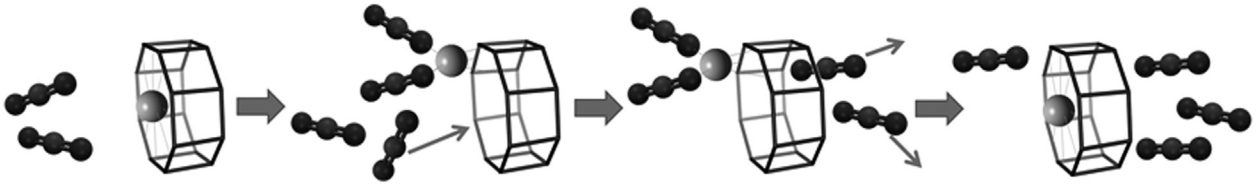

Fig. 1: Schematic representation of the trapdoor mechanism for CO_2 adsorption past cations in D8R window sites. 'Solvation' by adsorbed CO_2 molecules allows cations in the 8Rs to move away from the window and allow other CO_2 molecules to pass.

[6] and K–, Rb– and Cs–chabazite [11, 12] are examples of the former, Na-, K-, and Cs-forms of zeolite Rho [7–10] are examples of the latter. The presence of D8R windows in zeolite Rho, together with the ability of its framework to distort strongly, allows the D8R sites to bind the cations more closely, and permits trapdoor behaviour to occur up to higher gas pressures.

The small pore zeolite paulingite (topology type **PAU**) [13–17] is one of the most complex zeolites [18] and has a remarkable framework structure that contains cages connected in some cases by 8Rs and in others by D8Rs. The body-centred structure (space group $Im\bar{3}m$) in its undistorted, maximum symmetry form, is built up from seven different tiling units: *d8r*, *lta*, *pau, gis, oto, phi* and *plg* (Figure 2).

All of the pore space is accessible through windows bounded by 8Rs or D8Rs. Along each edge of the cubic unit cell there is a *lta-d8r-pau-d8r-pau-d8r-lta* sequence of cages, which connect at the *lta* sub-unit to give a 6-connected arrangement, in which the pore space is connected through D8R windows (Figure 3).

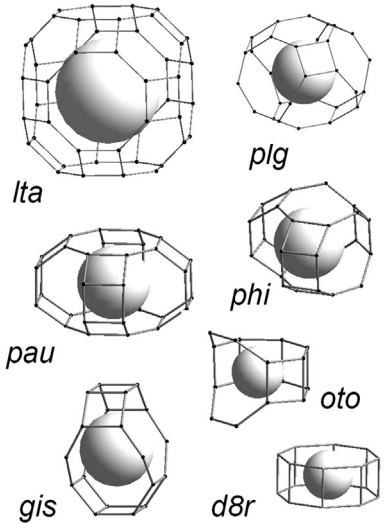

Fig. 2: Cages present in paulingite. Lines indicate T-T connectivity, with O atoms omitted for clarity. White spheres shown to illustrate cavity sizes, with radius of spheres shown as follows: *lta*, 4 Å; *plg, phi, pau, gis*, 3 Å; *d8r, oto*, 2 Å.

An identical 6-connected scaffold interpenetrates this one, as dictated by the body-centred symmetry. The region between these two interpenetrating arrangements of tiling units is built from *gis*, *oto*, *phi* and *plg* cages, all connected by 8R windows. The connection of tiling units along the <111> and <110> directions is shown in Figure 3. The two regions, volume A (*lta, d8r, pau*) and volume B (*gis, oto, phi, plg*) are linked, one to the other, via the 8R openings in the *pau* cages. Since the paulingite framework contains around 50% free space, all accessible via 8Rs, this suggests that the cationic forms of synthetic paulingite (ECR-18) can be selective, high capacity carbon capture adsorbents.

Although the crystal structure of the hydrated form of the mineral paulingite [14–17] and its partially dehydrated

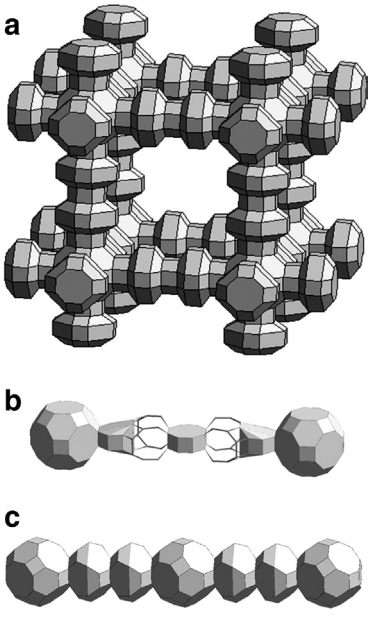

Fig. 3: (a) Polyhedral representation of the arrangement of *lta-d8r-pau-d8r-pau-lta* tiling units along unit cell edges of the **PAU** topology. A second, interpenetrating, set of such tiling units is also present in the body-centred topology, and the space in between the two is made up by *plg*, *phi*, *gis* and *oto* tiles. (b) Representation of *lta-oto-phi-d8r-phi-oto-lta* tiling units along the unit cell face diagonal of **PAU**. c) Representation of *lta-plg-plg-lta-plg-plg-lta* tiling units along the unit cell body diagonal of **PAU**.

form, unit cell composition $Ca_{59}K_{36}Na_{14}Ba_2[Si_{499}O_{1344}]$ [19, 20] have been reported, there have been no reports of the structure of the calcined synthetic paulingite, ECR-18. Measurements on dehydrated single crystals of the mineral have shown a decrease in unit cell parameter and associated distance least squares geometric modelling [19] indicated that the framework distorts to lower the symmetry to $I\bar{4}3m$, with the D8R units showing distortions similar to those observed experimentally for zeolite Rho. This has been confirmed by the single crystal structure of the partially dehydrated mineral [20]. In zeolite Rho, the cationic forms also change symmetry from $Im\bar{3}m$ to $I\bar{4}3m$ upon dehydration as the structure distorts to coordinate the cations more closely [6–10, 21, 22].

Here we report the Rietveld refinement of the structure of a dehydrated Na,H-form of ECR-18, along with its CO_2 adsorption behaviour. The composition was chosen as a compromise between pore volume and stability. H^+ is small and takes up little pore space but the ECR-18 structure is unstable in the fully protonated form, prepared by calcining a fully NH_4^+-exchanged ECR-18. The Na^+ form was chosen because the Na-form of Rho has been found to display interesting adsorption properties [8, 9]. The CO_2 adsorption is discussed in terms of the location of the Na^+ cations and intriguing *in situ* PXRD results during CO_2 adsorption are presented.

Experimental

The synthesis of ECR-18 (synthetic paulingite) was achieved by a hydrothermal route reported and confirmed in the literature [23, 24]. In a typical preparation, potassium hydroxide (1.79 g, 31 mmol, 99% Sigma Aldrich), sodium hydroxide (2.8 g, 70 mmol, 99% Fischer Scientific), aluminium isopropoxide (13.35 g, 65.36 mmol, 99% Aldrich) and water (8.0 g) were mixed and heated to reflux until a clear solution was formed (solution 1), and allowed to cool to room temperature. Then aluminium sulfate octadecahydrate (10 g, 15 mmol, Analar) and water (10 g) were mixed to form solution 2. Finally, silica solution (40%, 49.7 g, Ludox), tetraethylammonium hydroxide (40%, 43.3 g, Sigma Aldrich), solution 1 (17.5 g), solution 2 (5.29 g) and water (19 g) were mixed vigorously for 72 h, giving a homogeneous gel of composition 0.4 K_2O: 1.4$(TEA)_2O$: 0.6 Na_2O: Al_2O_3: 9SiO_2: 140H_2O. The mixture was then transferred to a Teflon-lined stainless steel autoclave and heated to 373 K for 16 days without agitation. After allowing the autoclave to cool to room temperature the product was filtered and washed with water yielding a white powder with spherical particles 2–3 microns in size. The as-prepared Na,K,TEA-ECR-18 was converted to Na,TEA-ECR-18 by rigorous ion exchange of K^+ with Na^+ using a 3 M aqueous solution of $NaNO_3$ over several days at 333 K, with the zeolite being separated by centrifugation and the $NaNO_3$ replaced with a fresh solution every day. EDX analysis was used to confirm complete replacement of K^+ by Na^+. The Na,H-form was prepared by calcination of the powder at 823 K under flowing oxygen to remove the TEA^+ cations present in the framework. CHN analysis confirmed all organic species had been removed. Inorganic analysis of Na,H-ECR-18 was carried out by EDX on a Jeol JSM 5600 SEM.

The crystallinity of cation-exchanged and calcined samples of ECR-18 was confirmed by laboratory PXRD using a Stoe STADI P diffractometer using Cu $K\alpha_1$ X-radiation (1.54056 Å). Thermogravimetry of cation-exchanged and calcined samples of ECR-18 was performed using a Netzsch TG 209 instrument with a heating rate of 5 K min^{-1} up to 1073 K in flowing air, in order to determine the temperature at which template removal or dehydration occurs (see Supporting Information). N_2 adsorption isotherms were measured volumetrically at 77 K using a Micromeritics Tristar II 3020 and performed between 0 and 1000 mbar. The CO_2 adsorption isotherm of the Na,H-form of ECR-18 over the pressure range of 0–900 mbar was measured volumetrically using an Autosorb iQ instrument, at 308 K. Prior to the experiment, the sample was evacuated overnight at 523 K to ensure that any physisorbed water was removed.

Solid-state ^{27}Al NMR spectra were obtained using a Bruker Avance III spectrometer, equipped with a 14.1 T wide-bore superconducting magnet (^1H Larmor frequency of 600.13 MHz). The samples were packed into a conventional 3.2 mm zirconia rotor, and rotated at a MAS rate of 20 kHz. A pulse of 1.25 μs ($\nu_1 \approx 100$ kHz) was applied. Signal averaging was carried out for 80 transients with a repeat interval of 3 s. Spectra were referenced to 1.1 M $Al(NO_3)_3$ in D_2O using solid $Al(acac)_3$ (δ_{iso} = 0 ppm, left hand horn = –1.1 ppm at 14.1 T) as a secondary reference.

Synchrotron powder X-ray diffraction was conducted at beamline I11 at the Diamond Light Source, Harwell [25]. A sample of zeolite was ground fine and packed into a 0.7 mm quartz glass capillary, using a quartz glass wool plug to keep it in place. The capillary was attached to the goniometer head of the gas cell [26] and the sample was evacuated and heated at 500 K for 2 h under a dynamic vacuum of 10^{-5} mbar to dehydrate it. The dehydrated sample was cooled to 298 K and kept under dynamic vacuum and the diffraction pattern collected using monochromated X-radiation (λ = 0.82696 Å) using a Mythen position sensitive detector, with a total scan time of 10 s. X-ray diffraction patterns were then collected as different pressures of CO_2 were allowed to come into contact with the dehydrated ECR-18 and adsorption was allowed to reach equilibrium over 20 min.

Rietveld refinement was performed for the dehydrated Na,H-form of ECR-18, prior to admission of CO_2. In order to obtain a starting model for the framework structure of dehydrated ECR-18, which shows a strong reduction in unit cell parameter compared to the hydrated material, a hypothetical pure silica framework was studied by molecular modelling. Simulation of the ECR-18 framework was conducted by refining the atomic positions of the ECR-18 structure using lattice energy minimisation within the program GULP [27], itself within the Materials Studio program (v6.0) [28]. The interatomic potentials used were those derived by Catlow et al. [29, 30]. A fully siliceous framework was assumed with the long-range electrostatic contribution to the lattice energy summed to infinity using the Ewald method. The unit cell parameters were held fixed during the course of the simulations and were performed with the values of the cubic cell parameter reduced stepwise from 33.0 Å to 31.5 Å. The initial model used atom positions derived from experimental studies in which the symmetry was $Im\bar{3}m$ [14] but assumed all tetrahedral cations were Si, because it would have been much more complicated to include a disordered arrangement of Al and Si. The unit cell parameters in the modelling were investigated over a range of values smaller than those observed experimentally because the Si–O bond lengths of the

model are smaller than those expected for the mean Si,Al–O bond lengths of the real material. No symmetry constraints were applied in the initial calculations and all the atoms were allowed to move independently (i.e. in *P*1). After the cell parameter dropped below 32.5 Å the symmetry of the minimised structure started to change from $Im\bar{3}m$. The new symmetry of the structure was assessed using the 'Find Symmetry' tool within the program Materials Studio (v6.0) [16], which showed that the new symmetry of the structure, within a tolerance of 0.4 Å, was $I\bar{4}3m$. The atomic positions were then adjusted so that all the atomic positions were consistent with the new $I\bar{4}3m$ space group and the final refinements within GULP were performed reducing the unit cell from 32.5 Å to 31.5 Å constraining the symmetry so that the $I\bar{4}3m$ space group was retained.

Results and discussion

Structural analysis

The unit cell parameter of the flexible zeolite ECR-18 was found to change significantly during cation exchange, dehydration and calcination (Table 1). Full cation exchange of K^+ by Na^+ results in a decrease of unit cell volume by 2.9% as smaller cations replace larger ones. The calcined, rehydrated material is again smaller, as the bulky organic cations are removed from cages in the structure.

Solid state ^{27}Al NMR of cation-exchanged Na, TEA-ECR-18 and calcined, hydrated Na,H-ECR-18 showed a single signal in each case, characteristic of tetrahedral Al within the framework structure. For the uncalcined sample, a relatively sharp resonance is observed with a maximum at 59.1 ppm, whereas the resonance for the calcined sample is slightly broader and shifted downfield, with a maximum at 62.0 ppm (see supporting information). This indicates that the framework remains intact upon calcination.

Fully dehydrated Na,H-ECR-18 has a unit cell composition, determined by EDX analysis, of $Na_{132}H_{28}Si_{512}Al_{160}O_{1344,}$ with a unit cell parameter of 33.3488(3) Å, a volume decrease of 12.7% compared to the calcined, hydrated Na,H-ECR-18. The framework with $I\bar{4}3m$ symmetry generated by lattice energy minimisation using the program GULP (see experimental section and Supporting information) was therefore used as a starting model for full Rietveld refinement using the GSAS suite of programs. [31] The measured Si/Al ratio was used for the framework cation composition in the refined structure, and kept constant. Na^+ cations were located by a combination of difference Fourier calculations and by refinement of occupancies and positions of cations placed in likely 8R sites. The positions and isotropic thermal parameters of framework atoms and extra framework cations were refined along with Na^+ cation positions: occupancies of Na^+ cations were also refined. Throughout, framework T–O and O–O bond distances were restrained, to 1.64 Å (tolerance 0.025 Å) and 2.64 Å (tolerance 0.05 Å), respectively. In the final refinement cycles all thermal parameters and atom positions were refined simultaneously (final restraint weight factor = 100) with the exception of 2 O atoms (O_{33} and O_{34}) and 2 T sites (T_{13} and T_{14}) which were each found to be oscillating between two positions, preventing convergence. These atoms were fixed so that the respective TO_4 tetrahedra had the most chemically reasonable of the possible positions. The occupancies of Na^+ cations were also refined. Atomic co-ordinates, isotropic thermal parameters and fractional occupancies obtained from the refined structure are given in the supporting information. A final fit of 1.84% was achieved using 19 Pseudovoigtian profile coefficients and

Tab. 2: Crystallographic details for the Rietveld refinement of dehydrated Na,H-ECR-18.

	Na,H-ECR-18 (dehydrated)
Measured chemical composition of unit cell	$Na_{132}H_{28}Al_{160}Si_{512}O_{1344}$
Chemical composition of unit cell from the refined structure	$Na_{127}Al_{160}Si_{512}O_{1344}$
Diffractometer	Synchrotron X-ray, I11, Diamond Light Source
Wavelength	0.82696 Å
Space group	$I\bar{4}3m$
a/Å	33.3488(3)
No. reflections	1106
No. parameters	194
R_p	0.0185
R_{wp}	0.0245
GOF	1.08

Tab. 1: Cubic unit cell parameters for ECR-18 materials in this study.

ECR-18 Form	**Code**	**Unit cell parameter (Å)**
As synthesised hydrated	Na,K,TEA-ECR-18·xH_2O	35.48707(2)
Na^+-exchanged hydrated	Na,TEA-ECR-18·xH_2O	35.13364(2)
Na^+-exchanged calcined hydrated	Na, H-ECR-18·xH_2O	34.89412(1)
Na^+-exchanged calcined dehydrated	Na,H-ECR-18	33.3488(3)

a 36 term shifted Chebyshev background function (Table 2 and Figure 4). Framework Si–O bond lengths and O–Si–O bond angles remained reasonable (see supporting information), the average bond length being 1.641(1) Å and the average angle being 109(5)°.

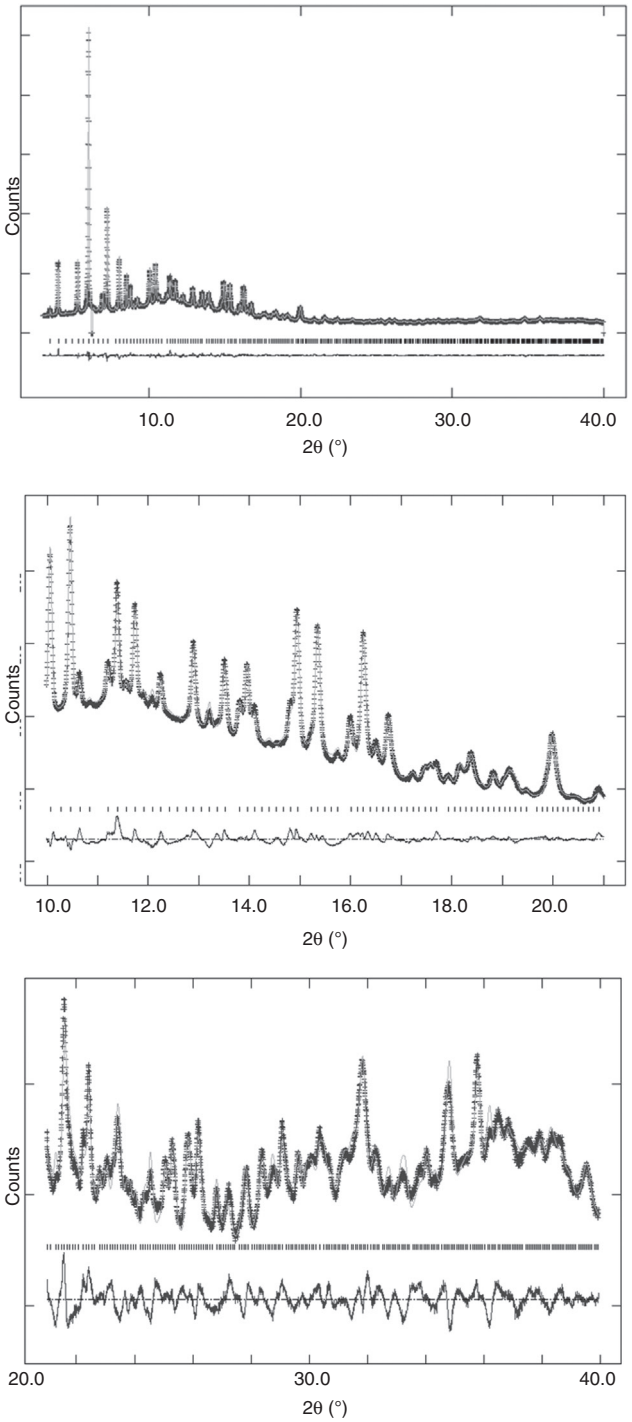

Fig. 4: Rietveld plots (synchrotron PXRD, λ = 0.826956 Å, T = 298 K) of dehydrated Na,H-ECR-18: (above) full range, and expanded (middle) 10–20°, and (below) 20–40°.

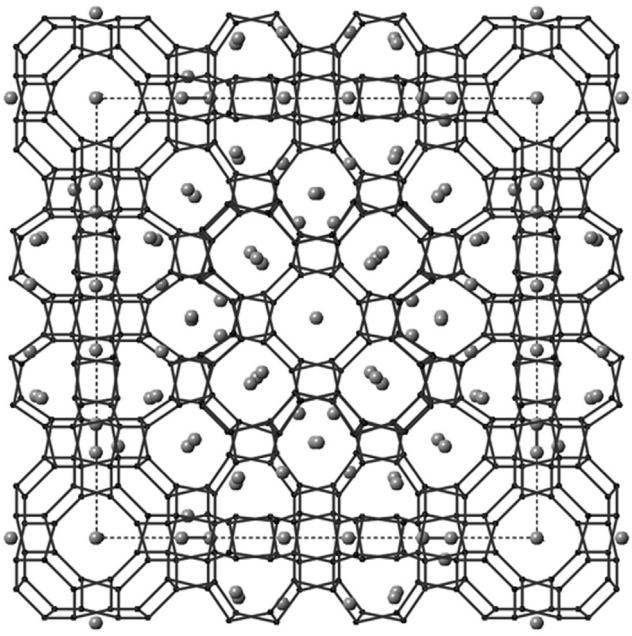

Fig. 5: Projection of structure of dehydrated Na,H-ECR-18 framework (O atoms omitted) with Na^+ cations positions shown (z = −0.25–0.25).

Upon calcination and dehydration the Na,H-ECR-18 structure distorts, and the space group symmetry changes from $Im\bar{3}m$ to $I\bar{4}3m$. The complexity of the PAU framework, together with the distortion, makes it difficult to represent the unit cell structure clearly. However, an overview of the positions of the Na^+ cation positions within the ECR-18 framework is given in the projection of a slice through the unit cell, from −0.25 to 0.25 in z, in Figure 5.

The framework distorts strongly from its original $Im\bar{3}m$ symmetry, so that, for example, the *lta* cages become markedly tetrahedral in shape and the *d8r* units distort strongly from being circular in cross section (Figure 6). Similar distortions in *lta* cages and *d8r*s are observed in dehydrated forms of cationic zeolite Rho. The

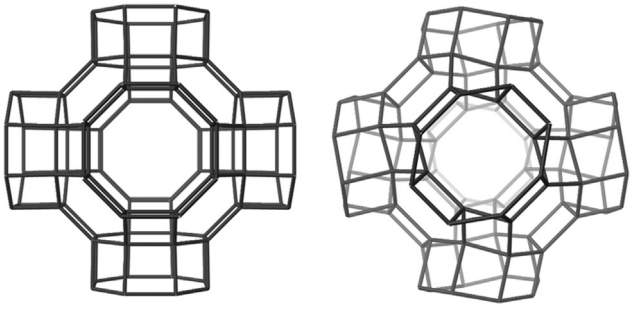

Fig. 6: Schematic representation of *lta* and *d8r* part of ECR-18 framework in (left) $Im\bar{3}m$ and (right) $I\bar{4}3m$ states, showing distortion from octahedral to tetrahedral geometry. Lines show T–T connectivity; O atoms omitted for clarity.

Tab. 3: Crystallographic details and description of location of Na+ cations in 8Rs of dehydrated Na,H-ECR-18, determined by Rietveld refinement.

Atom Name[a]	Fractional coordinates			Frac. Occup.	Mult.	No./unit cell	Location of 8R	Short Na-O distances[b] (Å)
	X	Y	Z					
NaA1	0.1949(20)	0	0	0.5	12	6	*lta/d8r*	2.81(2) (× 2)
NaA2	0.2941(20)	0	0	0.5	12	6	*d8r/pau*	2.81(2) (× 2)
NaA3	0.5684(23)	0	0	0.399(21)	12	4.8	*pau/d8r*	2.484(12) (× 2)
NaB1	0.2394(8)	0.2394(8)	−0.0336(13)	0.658(19)	24	15.8	*plg/oto*	2.521(14) (× 2) 3.05(4) (× 1)
NaB2	0.0457(8)	0.2040(6)	0.2040(6)	1	24	24	*plg/oto*	2.578(7) (× 2) 2.938 (× 2)
NaB3	0.3235(12)	0.1246(9)	0.1246(9)	0.647(20)	24	15.5	*pau/oto*	2.44(4) (× 1)
NaB4	0.3740(20)	0.3740(20)	0.1609(26)	0.296(20)	24	7.1	*plg/oto*	2.64(6) (× 2) 2.73(4) (× 2)
NaB5	0.0666(7)	0.4984(14)	0.2138(10)	0.549(12)	48	26.4	*phi/gis*	2.52(5) (× 1) 2.30(4) (× 1)
NaB6	0.3519(7)	0.3519(7)	0.0885(8)	0.895(19)	24	21.5	*phi/oto*	2.484(14) (× 1) 2.86(4) (× 1)

[a]A or B in atom label refers to Na^+ location in volume A or B of pore structure (as defined in text).
[b]Na-O distances < 3.05 Å are given.

Na^+ cations occupy 8R sites that are either present in 8R or D8R windows between cages (Table 3 and Figure 7). In the region of pore space we have described as volume A, all Na^+ cations are in 8R sites that are part of D8R windows (*lta-d8r-pau*) whereas in volume B (*plg, gis, phi, oto*) the Na^+ cations are in S8R sites that are part of 8R windows. Molecular transport between the two volumes is through 8R windows occupied by Na^+ cations.

The Na^+ cation positions are very similar to those of the K^+ cations (taken to be representative of all cations in the mineral) and water molecules previously reported in a partially dehydrated structure of natural paulingite [20]. In both structures the extra framework atoms are found to favour the 8R sites that are present throughout the structure of paulingite. The only site which contains extra framework atoms in the natural paulingite sample but not

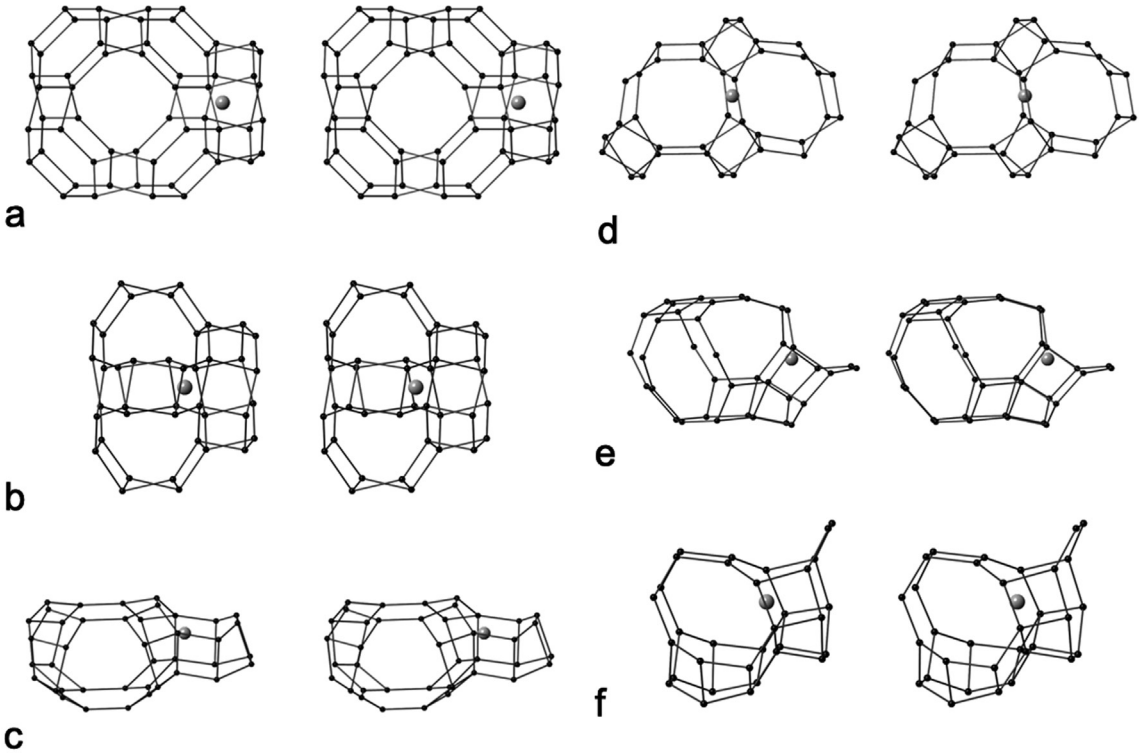

Fig. 7: Schematic stereoview representations of locations of Na^+ cations in 8R sites between cages. In some cases there is more than one symmetry inequivalent cation in a similar location, but the positions are very similar. Representative examples are shown (specific cation shown in bold): (a) *lta/d8r*: **NaA1**, (b) *pau/d8r*: **NaA2** and NaA3, (c) *pau/oto*: **NaB3**, (d) *phi/gis*: **NaB5**, (e) *plg/oto*: **NaB1**, NaB2, NaB4, and (f) *phi/oto*: **NaB6**.

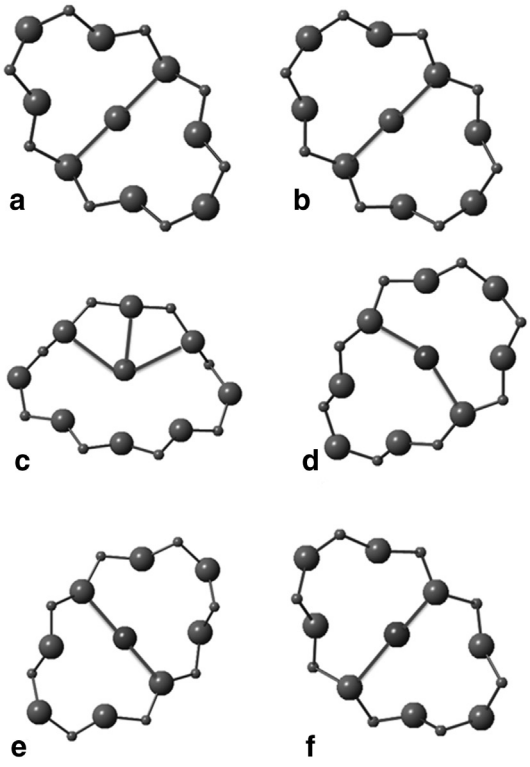

Fig. 8: Examples of Na^+ in 8R sites between cages, showing Na–O distances < 3.05 Å. (a) *lta*/*d8r* for cation NaA1, (b) *d8r/pau* for NaA2, (c) *plg/oto* for NaB1, (d) *pau/oto* for NaB3, (e) *phi/gis* for NaB5, (f) *phi/oto* for NaB6.

in the Na-ECR-18 is a 6R site occupied by a Ca^{2+} cation, and two partially occupied water sites, whereas NaB5 is the only occupied site in the Na-ECR-18 which does not correspond to any extra-framework atoms reported for the natural paulingite.

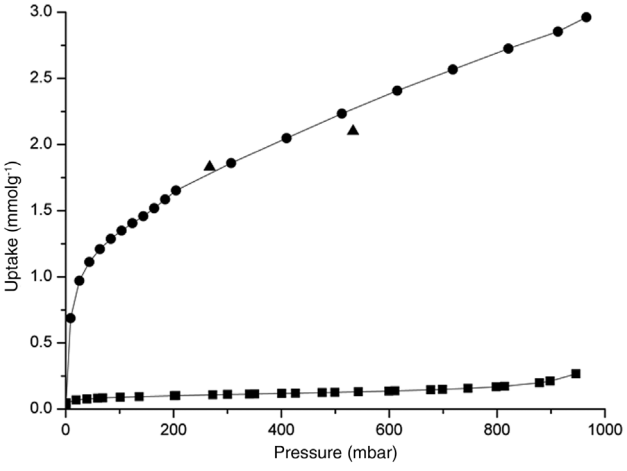

Fig. 9: Gas adsorption data for Na,H,-ECR-18 (squares, N_2 at 77 K; circles, CO_2 at 308 K), compared with literature adsorption data for Na, K-ECR-18 (triangles, CO_2 at 298 K) [22].

The presence of the Na^+ cations causes the distortion exhibited by the framework. Na^+ cations have a relatively small ionic radius and cannot easily achieve close Na^+–O^{2-} (framework) distances to more than one or two O atoms in undistorted 8R sites. However, by ellipical distortion of the 8Rs additional short and strong Na^+–O^{2-} bonds can be made (illustrated in Figure 8 for Na^+ in 8R sites in 8R units). The favourable electrostatic interactions achieved in this way offset the strain energy required to undergo the framework distortion, as seen previously for zeolite Rho [7–10, 21, 22].

Gas adsorption and in situ PXRD studies

Dehydrated Na,H-ECR-18 shows no porosity for N_2 at 77 K, despite the free volume present in the structure (Figure 9). This can be explained by the presence of Na^+ cations in all 8R windows between cages that block access of the N_2 molecules. These cations are unable to move because of the low temperature and their weak interaction with N_2 molecules. Without further investigation, the zeolite might have been considered non-porous. However, it takes up reasonable quantities of CO_2 at 308 K, when compared to other zeolites and microporous inorganic solids [1, 2]. The CO_2 uptake values are similar to those reported previously for calcined as-prepared ECR-18 (Na,K,TEA-ECR-18) [23]. The CO_2 uptake indicates that the CO_2 gas molecules must interact strongly with Na^+ cations in the 8R windows of ECR-18, drawing them out of their positions blocking the windows and creating an opening large enough for other CO_2 molecules to pass through the 8Rs into the neighbouring cage. This mechanism for gas separation has been called a trapdoor mechanism [8, 9, 11]. It permits adsorptive discrimination based on the magnitude of the interactions between different gas molecules and the gating cations, rather than the relative sizes of the molecules.

The structure of ECR-18 is such that for diffusion of molecules within the *lta-d8r-pau-d8r-pau-lta* regions the CO_2 must pass by Na^+ cations in D8R sites, as in Rho. In zeolite Rho this is found to result in slow diffusion because the pore space is only accessible via diffusion through vary many D8Rs [8, 9]. However, for diffusion through the volume containing *plg, oto, phi* and *gis* cages all Na^+ cations are in 8R window sites, where they might not be so strongly held. It might then be possible that the rate-determining step will be diffusion through this region of pore space (and then to the *lta/d8r/pau* region), and so might be faster.

The total amount of CO_2 taken up by Na,H–ECR-18 at 1 bar is moderate compared to that on zeolite Na–Rho.

This suggests inaccessibility of some cages, possibly due to the strong distortion. Synchrotron X-ray powder diffraction was therefore carried out *in situ* during the adsorption of CO_2 on the sample to determine whether structural changes occur (Figure 10). Upon exposure to increasing CO_2 gas pressure from 0 to 10 bar, the unit cell of the zeolite expanded continuously from 33.3488(3) Å (dehydrated) to 34.271 Å (10 bar CO_2), with the steepest increase in the region of sharpest rise in equilibrium uptake. The final value did not reach the value of 34.894 Å observed for hydrated Na,H-ECR-18, indicating that water molecules bind more strongly and pack more efficiently than CO_2 molecules. More remarkably, the diffraction patterns show strong broadening effects, which are significant from 0 to 1 bar and increase at higher pressures. Although this prevents structural refinement, it suggests that there is uneven distribution of strain in the zeolite structure.

To study the structural change which occurs in the sample upon exposure to high CO_2 pressures a series of diffraction patterns was collected at regular intervals (every 30 s) as the dehydrated sample was exposed to 10 bar of CO_2 (Figure 11). Once the system had equilibrated the sample was then exposed to vacuum again to remove the CO_2 and subsequently re-pressurised to 10 bar and the diffraction pattern monitored as before. The peak broadening at high CO_2 pressure is observed to be reversible upon exposure to vacuum, because the pattern rapidly changes back to have peak widths similar to those of the fully dehydrated pattern and the peak broadening is observed as before. This reversibility suggests the peak broadening results from strain rather than changes in the particle size. Furthermore the diffraction patterns suggest the changes in 'crystallinity' are occurring over a fast timescale (of the order of 2 min). We speculate that the changes in structure involve local distortion of the structure, rather than bond breaking.

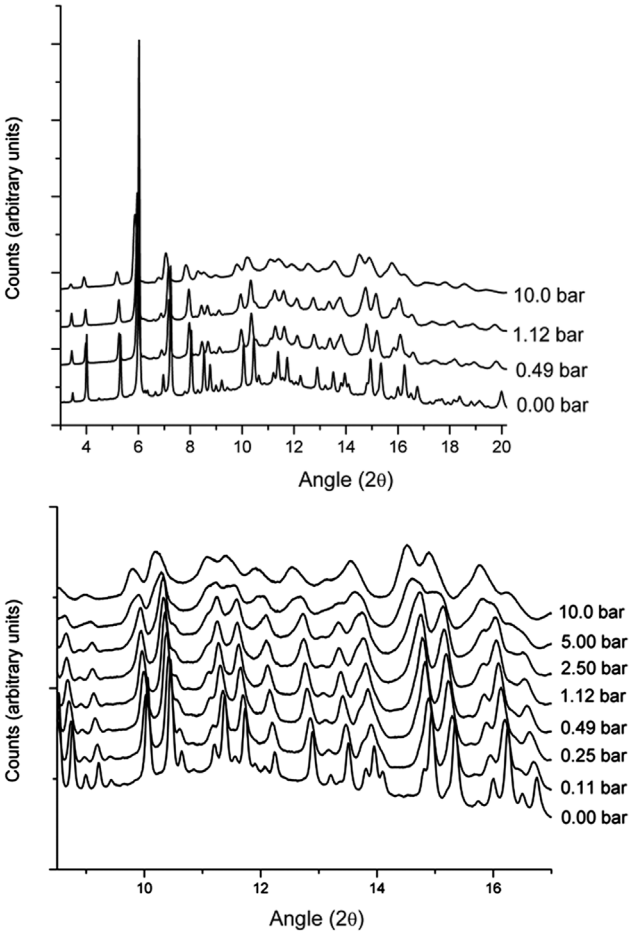

Fig. 10: PXRD patterns of Na,H,-ECR-18 measured *in situ* as a function of equilibrium CO_2 gas pressure. (Above) Diffraction patterns at different gas loading pressures, (below) expansion of part of diffraction patterns showing peak broadening upon exposure to CO_2 at different pressures.

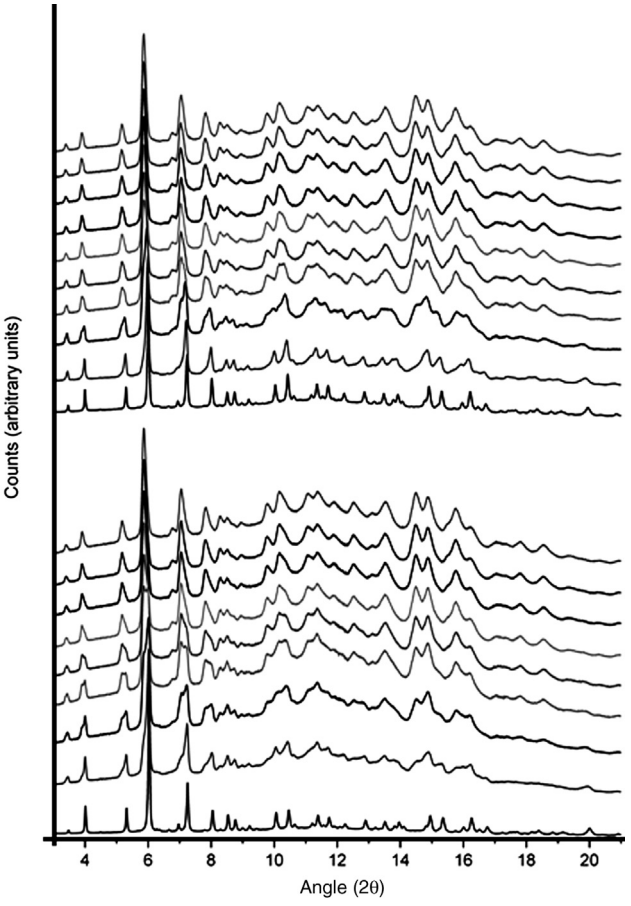

Fig. 11: Series of synchrotron X-ray powder diffraction patterns collected at intervals of 30 s showing rapid reversible changes of the ECR-18 framework in response to exposure to 10 bar CO_2 pressure (0–10 bar, twice).

Conclusion

We report the structure of dehydrated Na,H-ECR-18, Rietveld refined against synchrotron PXRD data. This has been achieved using as a starting model a framework structure determined by lattice energy minimisation to possess $I\bar{4}3m$ symmetry, in agreement with earlier DLS modelling. Sodium cations are found to occupy 8R sites throughout the complex framework, which are the windows between interconnected *lta*, *d8r*, *pau*, *oto*, *phi*, *gis* and *plg* cages in the open structure, and the distortion from $Im\bar{3}m$ to $I\bar{4}3m$ symmetry is a result of framework distortion to coordinate these Na^+ cations better within the 8Rs.

Gas adsorption studies have shown that Na,H-ECR-18 adsorbs no N_2 at 77 K, which is attributed to pore blocking by Na^+ cations in 8R window sites, but it does take up CO_2 at 308 K, a property that can be rationalised via a 'trapdoor' cation gating mechanism. More detailed experiments of the kinetics of N_2 adsorption at higher temperature (273 K and above) are required to evaluate ECR-18 for separation, in particular in mixtures with CO_2, and these are underway. Nevertheless, ECR-18 offers an alternative potential trapdoor zeolite that may be chemoselective for CO_2 in mixtures with N_2 and other less polar gases.

During CO_2 adsorption, the unit cell is observed to expand, and the powder diffraction pattern broadens reversibly, which we attribute to local strain within the crystals, rather than bond breakage. Given the broad peaks observed, a detailed understanding of the structural changes in this ECR-18 material might better be achieved by short range methods, such as pair distribution function analysis.

Acknowledgments: We thank the EPSRC (AMPgas, EP/J02077X/1; AGG, PAW, ES, SB), Diamond Light Source for beam time on stations I11 (EE9027-1) and Professor C. C. Tang for assistance at I11. S.B.H. acknowledges financial support from the NCRI (2012R1A3A-2048833) and BK 21-plus programs through the National Research Foundation of Korea.

References

[1] D. M. D'Alessandro, B. Smit, J. R. Long, *Angew. Chem. Int. Ed.* **2010**, *49*, 6058.
[2] G. Sneddon, A. Greenaway, H. H. P. Yiu, *Adv. Energy Mater.* **2014**, *4*, 1301873.
[3] M. Tagliabue, D. Farrusseng, S. Valencia, S. Aguado, U. Ravon, C. Rizzo, A. Corma, C. Mirodatos, *Chem. Eng. J.* **2009**, *155*, 553.
[4] G. D. Pirngruber, P. Raybaud, J. Cejka, A. Zukal, *Phys. Chem. Chem. Phys.* **2010**, *12*, 13534.
[5] M. Palomino, A. Corma, F. Rey, S. Valencia, *Langmuir* **2010**, *26*, 1910.
[6] Q. L. Liu, A. Mace, Z. Bacsik, J. L. Sun, A. Laaksonen, N. Hedin, *Chem. Commun.* **2010**, *46*, 4502.
[7] M. Palomino, A. Corma, J. L. Jordá, F. Rey, S. Valencia, *Chem. Commun.* **2012**, *48*, 215.
[8] M. M. Lozinska, E. Mangano, J. P. S. Mowat, A. M. Shepherd, R. F. Howe, S. P. Thompson, J. E. Parker, S. Brandani, P. A. Wright, *J. Am. Chem. Soc.* **2012**, *134*, 17628.
[9] M. M. Lozinska, J. P. S. Mowat, P. A. Wright, S. P. Thompson, J. L. Jorda, M. Palomino, S. Valencia, F. Rey, *Chem. Mater.* **2014**, *26*, 2052.
[10] M. Pera-Titus, M. Palomino, S. Valencia, F. Rey, *Phys. Chem. Chem. Phys.* **2014**, *16*, 24391.
[11] J. Shang, G. Li, R. Singh, Q. Gu, K. M. Nairn, T. J. Bastow, N. Medhekar, C. M. Doherty, A. J. Hill, J. Z. Liu, P. A. Webley, *J. Am. Chem. Soc.* **2012**, *134*, 19246.
[12] J. Shang, G. Li, R. Singh, P. Xiao, J. Z. Liu, P. A. Webley, *J. Phys. Chem. C* **2013**, *117*, 12841.
[13] E. K. Gordon, S. Samson, W. K. Kamb, *Science* **1966**, *154*, 1004.
[14] IZA-SC Database of Zeolite Structures, Ch. Baerlocher and L.B. McCusker, Database of Zeolite Structures: http://www.iza-structure.org/databases/.
[15] A. Bieniok, W. Joswig, W. H. Baur, *Neues. Jahrbuch. Miner.* **1996**, *171*, 119.
[16] C. L. Lengauer, G. Giester, E. Tillmanns, *Mineral. Mag.* **1997**, *61*, 591.
[17] A. E. Lapshin, O. V. Magdysyuk, O. Yu. Golubeva, E. A. Nikolaeva, *Glass Phys. Chem.* **2011**, *37*, 72.
[18] S. V. Krivovichev, *Angew. Chem. Int. Ed.* **2014**, *53*, 654.
[19] A. Bieniok, *Neues Jb. Miner. Monat.* **1997**, *11*, 498.
[20] A. Bieniok, *Natural Zeolites for the Third Millennium*, (Eds. C. Colella and F. A. Mumpton), DeFrede Editore Napoli, Italy, p. 53, **2000**.
[21] J. B. Parise, L. Abrams, T. E. Gier, D. R. Corbin, J. D. Jorgensen, E. Prince, *J. Phys. Chem.* **1984**, *88*, 2303.
[22] D. R. Corbin, L. Abrams, G. A. Jones, M. M. Eddy, W. T. A. Harrison, G. D. Stucky, D. E. Cox, *J. Am. Chem. Soc.* **1990**, *112*, 4821.
[23] D. E. W. Vaughan, K. G. Strohmaier, *Micropor. Mesopor. Mater.* **1999**, *28*, 233.
[24] D. J. Kim, C.-H. Shin, S. B. Hong, *Micropor. Mesopor. Mater.* **2005**, *83*, 319.
[25] S. P. Thompson, J. E. Parker, J. Potter, T. P. Hill, A. Birt, T. M. Cobb, F. Yuan, C. C. Tang, *Rev. Sci. Instrum.* **2009**, *80*, 075107.
[26] J. E. Parker, J. Potter, S. P. Thompson, A. R. Lennie, C. C. Tang, *Mater. Sci. Forum* **2012**, *706–709*, 1707.
[27] J. D. Gale, A. L. Rohl, *Mol. Simul.* **2003**, *29*, 291.
[28] Materials Studio, version 6.0, Accelrys Inc, San Diego, USA, **2012**.
[29] C. R. A. Catlow, R. James, W. C. Mackrodt, R. F. Stewart, *Phys. Rev. B: Condens. Matter.* **1982**, *25*, 1006.
[30] M. J. Sanders, M. Leslie, C. R. A. Catlow, *J. Chem. Soc. Chem. Comm.* **1984**, *19*, 1271.
[31] A. C. Larson, R. B. Von Dreele, *General Structure Analysis System (GSAS)*, Los Alamos National Laboratory, Los Alamos, **1994**.

Supplemental Material: The online version of this article (DOI: 10.1515/zkri-2014-1824) offers supplementary material, available to authorized users.